Supporting Information

Boosting Catalytic Oxidation of Ethane over Ce-Doped Ru/Co_3O_4: Cooperation of Electron-Rich Ru and Oxygen Vacancies

Yongxue An, [ab] Yunchong Wang, [ab] Haolong Huang, [ab] Yanfei Zheng, [ab] Cangpeng Shan, [ab] Tianao Zhang, [ab] Rui Han, [ab] Qian Zhao,*[ab] and Qingling Liu*[ab]

[a] Tianjin Key Lab of Indoor Air Environmental Quality Control, School of Environmental Science and Engineering, Tianjin University, Tianjin 300350, China

[b] State Key Laboratory of Engines, Tianjin University, Tianjin 300350, China

Corresponding author: zhao_q@tju.edu.cn,

liuql@tju.edu.cn

CONTENTS

Text S1 Materials and methods

The catalyst slurry was prepared via a ball milling method. Typically, 2.5 g of the as-prepared Ru/0.1Ce-Co_3O_4 powder, 7.25 g of deionized water, and 0.25 g of 20 wt.% aluminum sol (Dezhou Jinghuo Technical Glass Co., Ltd.) were added together and mixed thoroughly. The resulting mixture was then transferred into a ball mill and milled for 12 h to obtain the catalyst slurry.

The monolithic catalyst was prepared via a coating method. Typically, cordierite support was immersed in the aforementioned catalyst slurry for 3 min. After being taken out, the excess slurry on the surface and within the pores of the cordierite support was thoroughly blown off. The coated cordierite was subsequently dried at 100 ℃ for 1 h, and finally calcined at 400 ℃ for 4 h to obtain the monolithic catalyst.

Text S2 Catalyst Characterization

The actual metal contents of catalysts were determined by Inductively Coupled Plasma Optical Emission Spectrometer technique (ICP-OES, Agilent 725 ES). N_2 adsorption-desorption tests were carried out using a physical adsorption analyzer (ASAP 2020 PLUS HD88, Micromeritics, USA) at a temperature of -196 ℃. The pore size distributions were calculated by Barrett–Joyner–Halenda (BJH) method. The Brunauer–Emmett–Teller (BET) model was used to analyze the surface area. X-ray diffraction (XRD) patterns were collected using a Rigaku MiniFlex600 diffractometer with Cu Kα radiation at 40 kV and 200 mA. Transmission electron microscopy (TEM, JEM-2100F, JEOL, Japan) and high-angle annular dark-field scanning transmission electron microscopy (HAADF-STEM, Themis Z, Thermo Scientific, USA) combined with energy-dispersive X-ray spectroscopy (EDS, Super-X four-detector system, Thermo Scientific, USA). Raman spectra was recorded on a confocal Raman microscope (inVia, Renishaw) with an excitation laser of 532 nm. X-ray photoelectron spectroscopy (XPS) experiments were conducted using a Thermo Fisher instrument (ESCALAB 250Xi) with Al-Kα as the radiation source. The binding energy of the carbon (C 1s) was set as 284.8 eV for calibrating the samples.

CO pluse chemisorption, temperature-programmed desorption of oxygen (O_2-TPD), temperature-programmed reduction in ethane (C_2H_6-TPR) and temperature-

programmed surface reaction of propane (C_2H_6-TPSR) were carried out on a BSD-Chem C200 instrument. Before the CO pluse chemisorption tests, 50 mg of sample was pretreated with He (30 mL/min) at 200 °C for 1 h. After cooling down to 50 ℃, pulse of 1 % CO balanced with He was injected to the sample and the precious metal dispersion was calculated on the basis of equation Ru/CO = 1/1 when the adsorption was complete. Before the O_2-TPD tests, 50 mg of sample was preheated with He (30 mL/min) at 300 ℃ for 1 h. After cooling down to 50 ℃, 10% O_2/He was introduced at 30 mL/min for 1h, then He was introduced at 30 mL/min for 1h, Finally, the desorption of O_2 from the sample was measured by heating the sample from 50 ℃ to 700 ℃ at a ramping rate of 10 ℃/min in He (30 mL/min). Before the C_2H_6-TPR tests, 50 mg of sample was preheated with He (30 mL/min) at 300 ℃ for 1 h. After cooling down to 50 ℃, 1000 ppm of C_2H_6/Ar (30 mL/min) was introduced into the reaction tube and heated to 600 ℃ at a rate of 10 ℃/min. Before the C_2H_6-TPSR tests, 50 mg of sample was preheated with Ar (30 mL/min) at 300 ℃ for 1 h. After cooling down to 50, 1000 ppm of C_2H_6/Ar (30 mL/min) was introduced at 30 mL/min for 1h, then Ar was introduced at 30 mL/min for 1 h. Finally, the surface reaction was measured by heating the sample from 50 ℃ to 900 ℃ at a ramping rate of 10 °C/min in 10% O_2/He (30 mL/min). Record the signals generated during the C_2H_6-TPR and C_2H_6-TPSR tests via mass spectrometry (Hiden HPR-20 R&D, England).

In-situ diffuse reflectance infrared Fourier transform spectroscopy (DRIFTS) was performed on a Bruker Tensor II spectrometer (Bruker) equipped with liquid nitrogen cooling (-196 ℃) and a high-sensitivity mercury cadmium telluride (MCT) detector. The sample was treated with nitrogen (15 mL/min) at 300 ℃ for 30 minutes and cooled to 50 ℃ to collect the background. Next, the sample was exposed to 1% CO/N_2 for 60 minutes. Finally, the sample was purged with N_2 for 60 minutes, and then the spectrum was recorded.

In-situ DRIFTS of ethane degradation was acquired using a Bruker Tensor II spectrometer (Bruker) equipped with liquid nitrogen cooling (-196 ℃) and a high-sensitivity mercury cadmium telluride (MCT) detector. The sample was pretreated in air at 300 ℃ for 1 h, then cooled to 50 ℃. After purging with N_2 for 30 minutes, a

background spectrum was collected under N_2. Following background acquisition at each temperature point, a gas mixture of 800 ppm C_2H_6/N_2 (total flow rate: 30 mL/min) was introduced into the chamber, and spectra were recorded simultaneously. The relevant tests are conducted by altering temperature and gas composition, with spectra recorded at each temperature point. DRIFT spectra were sequentially acquired by accumulating 64 scans at a spectral resolution of 4 cm^{-1}.

Text S3 Catalytic Activity Evaluation

The conversion rate of ethane (X) and the yield of CO_2 (Y) are evaluated through the following equations:

$$X = \frac{c_{in} - c_{out}}{c_{in}} \times 100\%$$

where c_{in} and c_{out} were ethane concentration before the reaction and after oxidation, respectively.

$$Y = \frac{c_{CO_2}}{c_{in}} \times 100\%$$

where c_{CO_2} was the concentration of CO_2 at various reaction temperature points.

The kinetic experiments were conducted under conditions of ethane conversion <20% with a gas hourly space velocity (GHSV) of 120000 mL/(g·h). The first-order kinetic equation is expressed as:

$$lnr = -E_a/RT + B$$

where r was reaction rate (mmol/(g·s)), calculated from ethane conversion, gas flow rate, and catalyst mass. E_a was apparent activation energy (kJ/mol), determined from the linear relationship between 1000/T and ln r.

The long-term stability experiment was tested at 260 ℃ for 60 hours. And the water resistance test was conducted at 320 ℃ and 220 ℃ for 36 hours in the presence of 10 vol.% water vapor.

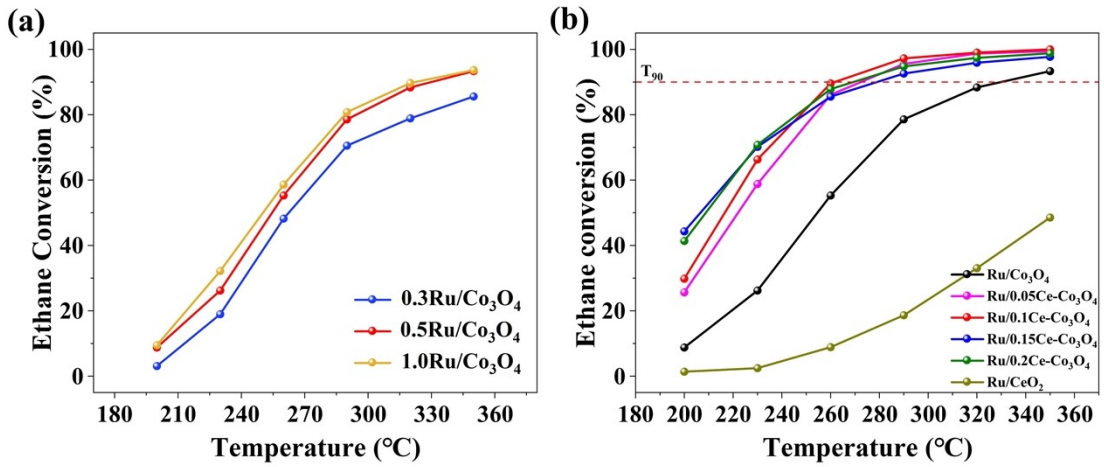

121

122 **Fig. S1** Ethane conversion of different (a) Ru contents of Ru/Co_3O_4 and (b) Ce contents

123 of $Ru/xCe\text{-}Co_3O_4$.

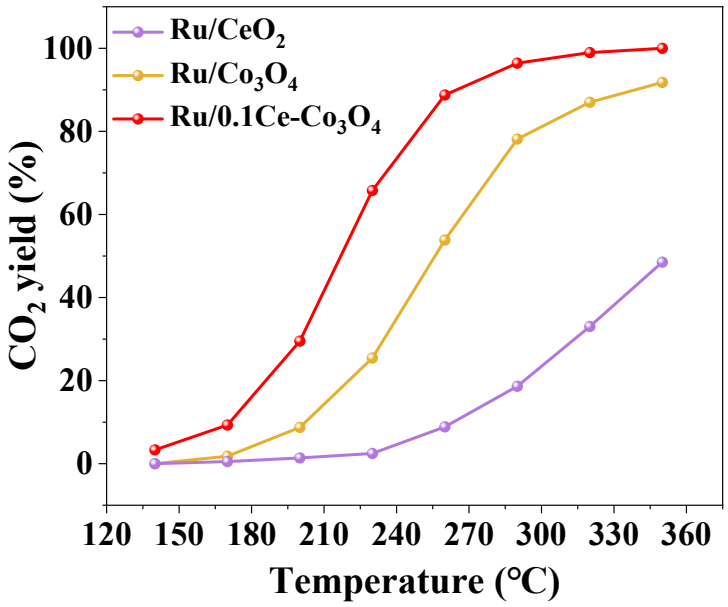

125

126 **Fig. S2** CO_2 yield of Ru/CeO_2, Ru/Co_3O_4 and $Ru/0.1Ce\text{-}Co_3O_4$.

127

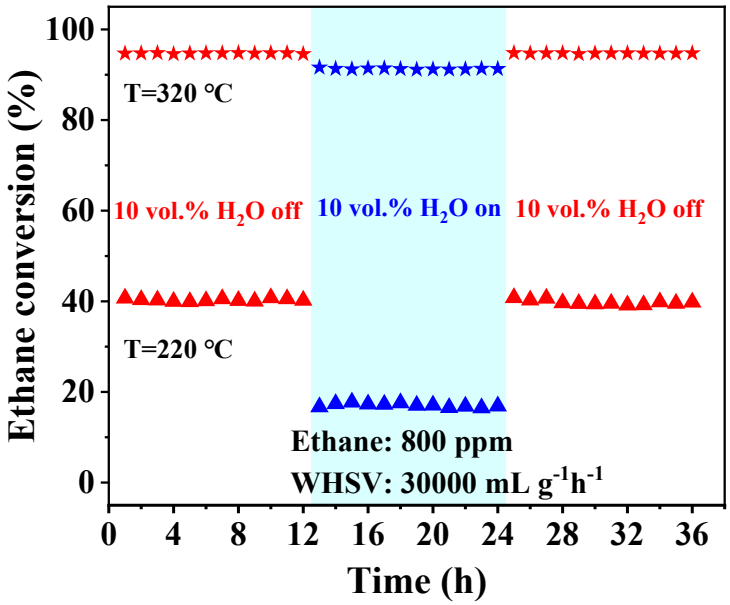

Fig. S3 Water resistance test of Ru/0.1Ce-Co_3O_4 in the presence of 10 vol.% H_2O.

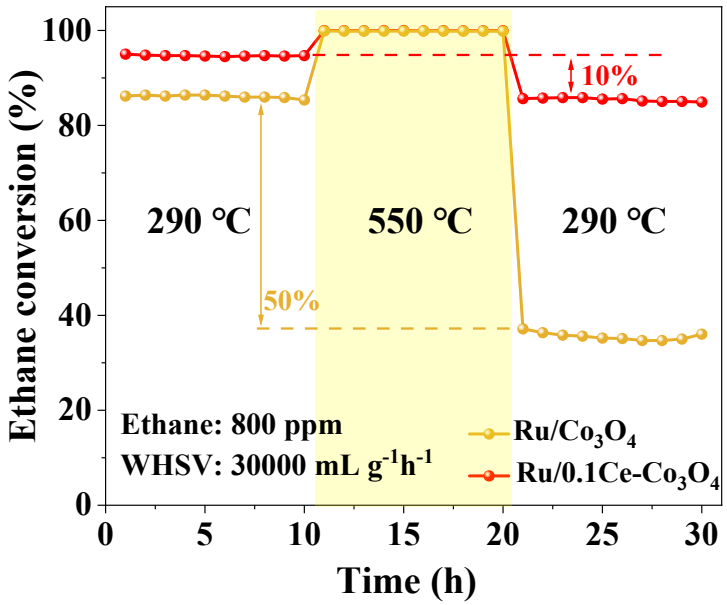

131

132 **Fig. S4** Stability test of high temperature shock on Ru/Co_3O_4 and $Ru/0.1Ce\text{-}Co_3O_4$ for

133 ethane oxidation.

134

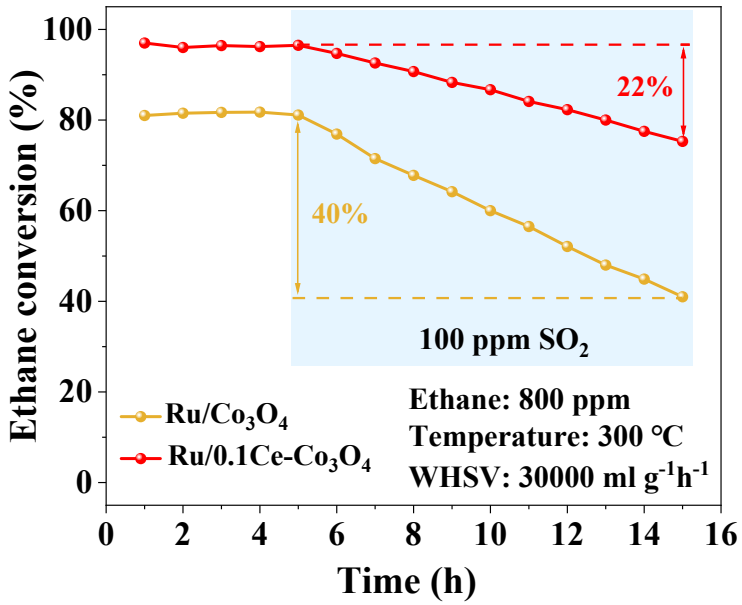

135

136 **Fig. S5** SO_2-tolerant tests on Ru/Co_3O_4 and $Ru/0.1Ce\text{-}Co_3O_4$ for ethane oxidation.

137

138

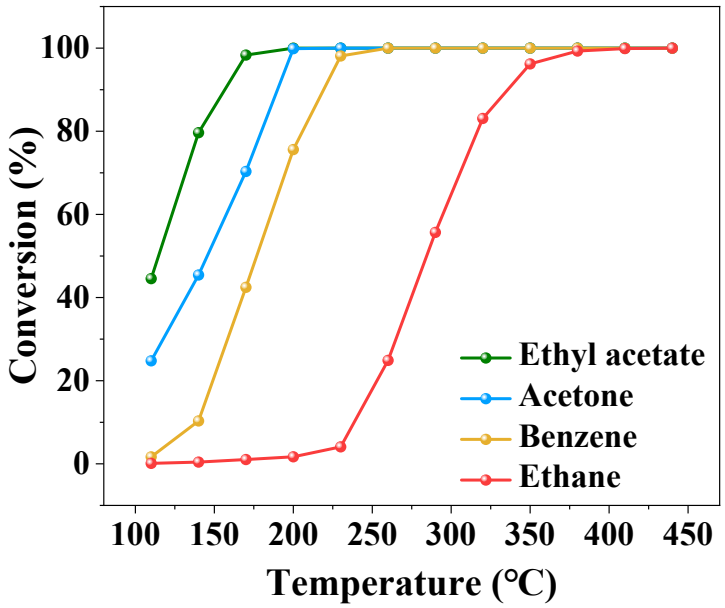

Fig. S6 Catalytic oxidation activity of VOCs on monolithic catalysts (VOCs of 800 ppm and GHSV of 12000 h^{-1}).

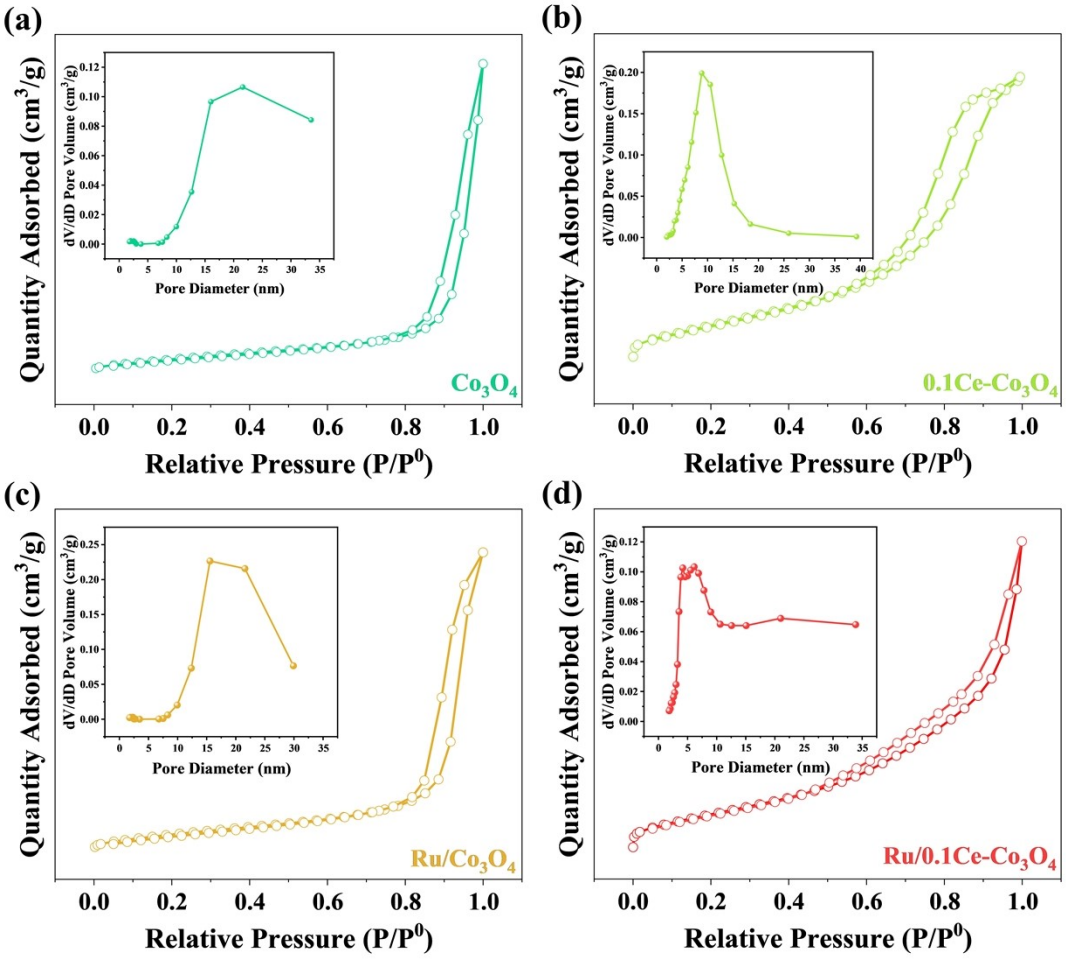

143

144 **Fig. S7** N_2 adsorption−desorption curve and pore diameter distribution of (a) Co_3O_4.

145 (b) 0.1Ce-Co_3O_4. (c) Ru/Co_3O_4 and (d) Ru/0.1Ce-Co_3O_4.

146

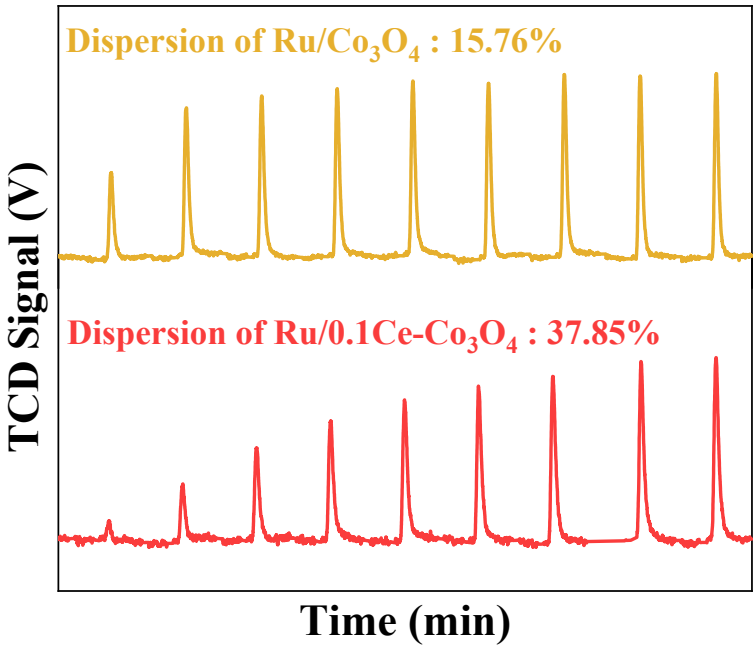

147

148 **Fig. S8** CO pulse patterns of Ru/Co_3O_4 and $Ru/0.1Ce\text{-}Co_3O_4$.

149

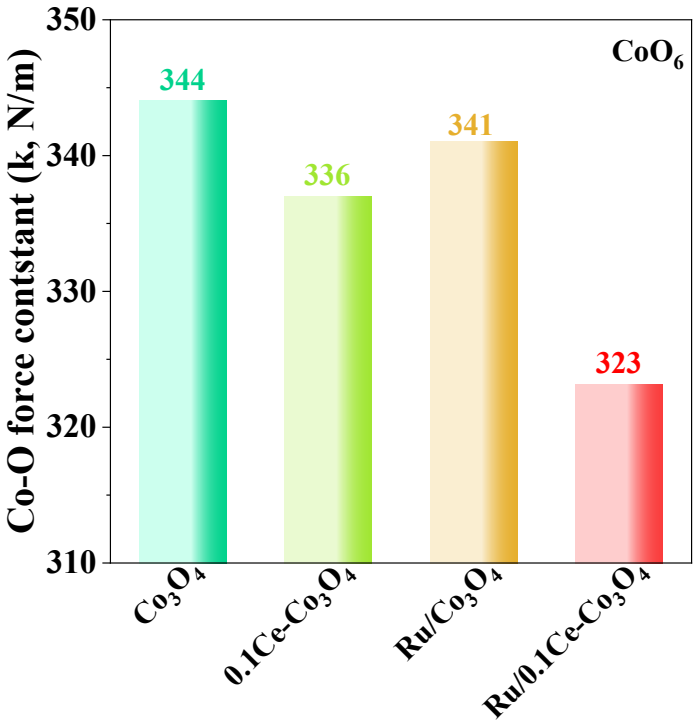

Fig. S9 The Co−O bond force constant (k) of CoO_6 in Co_3O_4, 0.1Ce-Co_3O_4, Ru/Co_3O_4 and Ru/0.1Ce-Co_3O_4.

The strength of the Co-O bond was further calculated according to Hooke's law[1]

$$\omega = \frac{1}{2\pi c} \cdot \sqrt{\frac{k}{\mu}}$$

Where k is the force constant of the Co-O bond, the more likely the Co−O bond will break. ω is the Raman shift (cm^{-1}), c is light velocity, and μ is effective mass.

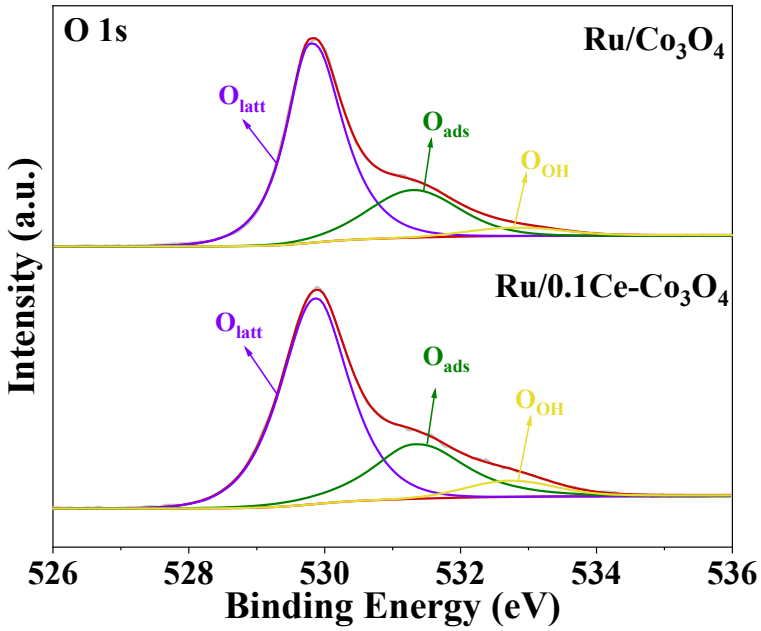

157

158 **Fig S10.** O 1s XPS spectra of Ru/Co_3O_4 and $Ru/0.1Ce\text{-}Co_3O_4$.

159

160 **Table S1** Catalytic activity for ethane oxidation over various catalysts

Catalysts	Gas feed composition	WHSV ($mL \cdot g_{cat}^{-1} \cdot h^{-1}$)	T_{90} (°C)	Refs.
$Ru/0.1Ce\text{-}Co_3O_4$	1000ppm C_2H_6+21% O_2/N_2	30000	260	This work
$NiCo_2O_4$-TM	3000ppm C_2H_6+11% O_2/N_2	48000	311	2
Fe_2O_3-S	2500 ppm C_2H_6+21% O_2/N_2	12000	415	3
$MnCoO_{x\text{-}0.5}$	3000ppm C_2H_6+11% O_2/N_2	60000	220	4
Pt/CZ11	1000ppm C_2H_6+21% O_2/N_2	50000	308	5
LMO@CMO-10	1000mg/m^3 C_2H_6+21% O_2/N_2	80000	341	6
$2\%Pd/\gamma\text{-}Al_2O_3$	10000ppm C_2H_6+10% O_2/He	187500	450	7
Au/CoOx	5000ppm C_2H_6+21% O_2/N_2	15000	230	8
$2Pd0.5Pt/Al_2O_3$	800ppm C_2H_6+21% O_2/N_2	100000	425	9
$La_{0.7}Bi_{0.3}Mn_{0.5}Co_{0.5}O_3$	2000ppm C_2H_6+21% O_2/N_2	12000	718	10
$Pt\text{-}Nb/ZrO_2$	0.3%C_2H_6+2%O_2+ 97.7%N_2	20000	280	11
$Pt/Ce_{0.01}Ti_{0.99}O_2$	1000ppm C_2H_6+4% O_2/N_2	60000	370	12
$La_{0.7}Sr_{0.3}Mn_{1\text{-}x}Co_xO_3$	6% CO+0.2% C_2H_6+20% O_2/Ar	12000	380	13
$Ce_{0.5}Mn_1$	500ppm C_2H_6+5% O_2/N_2	40000	320	14

161

Sample	D[a] (nm)	S_{BET} [b] (m^2/g)	V_{total} [c] (cm_3/g)	D_{pore} [d] (nm)	Ru content (wt%)	Ce:Co Metal molar ratio
Co_3O_4	21.0	26.60	0.13	20.39	/	/
0.1CeCo	8.0	76.71	0.17	8.34	/	0.11:1
Ru/Co_3O_4	20.3	48.12	0.20	17.55	0.49	/
$Ru/0.1Ce\text{-}Co_3O_4$	7.5	107.32	0.22	8.28	0.48	0.10:1

Table S2 Physical properties of catalysts.

[a] Calculated from the cobalt (220), (311), and (400) planes based on the Scherrer equation.

[b] Surface area by the Brunauer-Emmett-Teller (BET) method.

[c] Total pore volumes of $P/P_0 = 0.95$.

[d] Average pore diameter (4 V/A).

Table S3 The results of XPS analysis.

Sample	O_{ads}:O_{latt}	Ru^0:Ru (%)	Ru^{n+}:Ru (%)	Ru^{4+}:Ru (%)
Ru/Co_3O_4	0.34	17.24	57.47	25.29
$Ru/0.1\ Ce\text{-}Co_3O_4$	0.39	27.61	61.35	11.04

Reference

1 S. Rong, P. Zhang, F. Liu and Y. Yang, *ACS Catal.*, 2018, **8**, 3435-3446.

2 S. Liu, H. Wang, S. Wang, Y. Dai, B. Liu, Y. Liu, F. Dang, K. J. Smith, X. Nie, S. Hou and X. Guo, *ACS Catal.*, 2023, **13**, 4683-4699.

3 Y. Jian, T. Yu, Z. Jiang, Y. Yu, M. Douthwaite, J. Liu, R. Albilali and C. He, *ACS Appl. Mater. Interfaces*, 2019, **11**, 11369-11383.

4 H. Wang, S. Wang, S. Liu, Y. Dai, Z. Jia, X. Li, S. Liu, F. Dang, K. J. Smith, X. Nie, S. Hou and X. Guo, *Nat. Commun.*, 2024, **15**, 4118-4133.

5 Q. Fu, S. Wang, T. Wang, D. Xing, X. Yue, M. Wang and S. Wang, *J. Catal.*, 2022, **405**, 129-139.

6 J. Qin, P. Zhao, J. Meng, S. Zuo, X. Wang, W. Zhu, W. Liu, J. Liu and C. Yao, *Appl. Surf. Sci.*, 2024, **653**, 159393-159402.

7 O. Demoulin, B. Le Clef, M. Navez and P. Ruiz, *Appl. Catal. A-Gen.*, 2008, **344**, 1-9.

8 B. E. Solsona, T. Garcia, C. Jones, S. H. Taylor, A. F. Carley and G. J. Hutchings, *Appl. Catal. A-Gen.*, 2006, **312**, 67-76.

9 Z. Ma, J. Zhou, J. Lin, G. Yang, S. Liu and G. Li, *Fuel*, 2024, **374**, 132437-132446.

10 A. Gholizadeh and A. Malekzadeh, *Int. J. Appl. Ceram. Technol.*, 2017, **14**, 404-412.

11 B. Cen, C. Tang, J. Lu, J. Chen and M. Luo, *Chin. J. Catal.*, 2021, **42**, 2287-2295.

12 D. Wu, X. Lv, X. Ren, C. Hou, Q. Ma, J. Yao and J. Hu, *Catalysts*, 2023, **13**, 626-640.

13 A. Gholizadeh, A. Malekzadeh and M. Ghiasi, *Ceram. Int.*, 2016, **42**, 5707-5717.

14 S. Du, J. Hu, J. Wang, S. Wang, J. Hou, J. Li, Y. Su, L. Chang, H. Qin, Y. Wang and W. Bao, *Fuel*, 2023, **350**, 128762-128772.